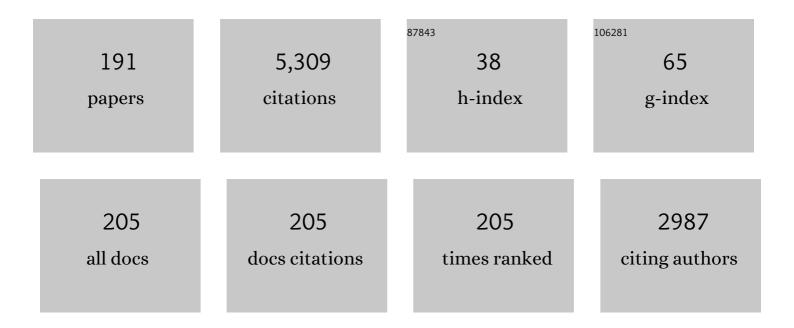
Wlodek Kofman

List of Publications by Year in descending order

Source: https://exaly.com/author-pdf/5623544/publications.pdf Version: 2024-02-01



#	Article	IF	CITATIONS
1	Subsurface Radar Sounding of the South Polar Layered Deposits of Mars. Science, 2007, 316, 92-95.	6.0	330
2	Radar Soundings of the Subsurface of Mars. Science, 2005, 310, 1925-1928.	6.0	327
3	The landing(s) of Philae and inferences about comet surface mechanical properties. Science, 2015, 349, aaa9816.	6.0	212
4	Properties of the 67P/Churyumov-Gerasimenko interior revealed by CONSERT radar. Science, 2015, 349, aab0639.	6.0	178
5	The Cluster Spatio-Temporal Analysis of Field Fluctuations (STAFF) Experiment. Space Science Reviews, 1997, 79, 107-136.	3.7	148
6	The Mars express MARSIS sounder instrument. Planetary and Space Science, 2009, 57, 1975-1986.	0.9	134
7	North polar deposits of Mars: Extreme purity of the water ice. Geophysical Research Letters, 2009, 36, .	1.5	129
8	The Comet Nucleus Sounding Experiment by Radiowave Transmission (CONSERT): A Short Description of the Instrument and of the Commissioning Stages. Space Science Reviews, 2007, 128, 413-432.	3.7	116
9	Estimation of the total electron content of the Martian ionosphere using radar sounder surface echoes. Geophysical Research Letters, 2007, 34, .	1.5	115
10	Dielectric map of the Martian northern hemisphere and the nature of plain filling materials. Geophysical Research Letters, 2012, 39, .	1.5	112
11	Elevated electron temperatures in the auroral <i>E</i> layer measured with the Chatanika Radar. Journal of Geophysical Research, 1981, 86, 4721-4730.	3.3	90
12	Comet nucleus sounding experiment by radiowave transmission. Advances in Space Research, 1998, 21, 1589-1598.	1.2	90
13	Accumulation and Erosion of Mars' South Polar Layered Deposits. Science, 2007, 317, 1715-1718.	6.0	84
14	The 3–5MHz global reflectivity map of Mars by MARSIS/Mars Express: Implications for the current inventory of subsurface H2O. Icarus, 2010, 210, 612-625.	1.1	82
15	TandEM: Titan and Enceladus mission. Experimental Astronomy, 2009, 23, 893-946.	1.6	77
16	Radar signal simulation: Surface modeling with the Facet Method. Radio Science, 2004, 39, n/a-n/a.	0.8	75
17	Impact of Mars ionosphere on orbital radar sounder operation and data processing. Planetary and Space Science, 2003, 51, 505-515.	0.9	70
18	Observations of aurorae by SPICAM ultraviolet spectrograph on board Mars Express: Simultaneous ASPERAâ€3 and MARSIS measurements. Journal of Geophysical Research, 2008, 113, .	3.3	70

#	Article	IF	CITATIONS
19	Small-Scale Plasma-Density Depletions in Arecibo High-Frequency Modification Experiments. Physical Review Letters, 1986, 57, 1008-1011.	2.9	68
20	Correction of the ionospheric distortion on the MARSIS surface sounding echoes. Planetary and Space Science, 2008, 56, 917-926.	0.9	68
21	Observations of enhanced plasma lines by EISCAT during heating experiments. Radio Science, 1983, 18, 861-866.	0.8	66
22	Mars Advanced Radar for Subsurface and Ionospheric Sounding (MARSIS) after nine years of operation: A summary. Planetary and Space Science, 2015, 112, 98-114.	0.9	66
23	Cosmochemical implications of CONSERT permittivity characterization of 67P/CG. Monthly Notices of the Royal Astronomical Society, 2016, 462, S516-S532.	1.6	59
24	RIME: Radar for Icy Moon Exploration. , 2013, , .		57
25	Direct observations of asteroid interior and regolith structure: Science measurement requirements. Advances in Space Research, 2018, 62, 2141-2162.	1.2	54
26	The Philae lander mission and science overview. Philosophical Transactions Series A, Mathematical, Physical, and Engineering Sciences, 2017, 375, 20160248.	1.6	53
27	Quantitative analysis of Mars surface radar reflectivity at 20MHz. Icarus, 2012, 220, 84-99.	1.1	52
28	Aspect angle dependence of HF enhanced incoherent backscatter. Advances in Space Research, 1999, 24, 1003-1006.	1.2	50
29	Radar properties of comets: Parametric dielectric modeling of Comet 67P/Churyumov–Gerasimenko. Icarus, 2012, 221, 925-939.	1.1	50
30	The WISDOM Radar: Unveiling the Subsurface Beneath the ExoMars Rover and Identifying the Best Locations for Drilling. Astrobiology, 2017, 17, 565-584.	1.5	50
31	Subsurface Radar Sounding of the Jovian Moon Ganymede. Proceedings of the IEEE, 2011, 99, 837-857.	16.4	49
32	Very high electron temperatures in the daytime F region at Sondrestrom. Geophysical Research Letters, 1984, 11, 919-922.	1.5	47
33	Proton transport model in the ionosphere: 1. Multistream approach of the transport equations. Journal of Geophysical Research, 1997, 102, 22261-22272.	3.3	46
34	Direct measurements of ion composition with EISCAT in the highâ€ŀatitude <i>F</i> ₁ region. Radio Science, 1983, 18, 887-893.	0.8	44
35	New phenomena observed by EISCAT during an RF ionospheric modification experiment. Radio Science, 1990, 25, 251-262.	0.8	44
36	A characterization of a comet nucleus interior:. Planetary and Space Science, 1999, 47, 885-904.	0.9	42

#	Article	IF	CITATIONS
37	Dielectric properties of comet analog refractory materials. Planetary and Space Science, 2002, 50, 857-863.	0.9	41
38	Incoherent scattering of an electromagnetic wave in the mesosphere: A theoretical consideration Journal of Geomagnetism and Geoelectricity, 1980, 32, 67-81.	0.8	40
39	Philae's First Days on the Comet. Science, 2015, 349, 493-493.	6.0	40
40	Incoherent scatter measurements of ionâ€neutral collision frequencies and temperatures in the lower the region. Journal of Geophysical Research, 1983, 88, 10137-10144.	3.3	38
41	CONSERT suggests a change in local properties of 67P/Churyumov-Gerasimenko's nucleus at depth. Astronomy and Astrophysics, 2015, 583, A40.	2.1	37
42	Assessing the potential for passive radio sounding of Europa and Ganymede with RIME and REASON. Planetary and Space Science, 2016, 134, 52-60.	0.9	36
43	Dayside red auroras at very high latitudes: The importance of thermal excitation. Geophysical Research Letters, 1984, 11, 923-926.	1.5	35
44	Natural radio emission of Jupiter as interferences for radar investigations of the icy satellites of Jupiter. Planetary and Space Science, 2012, 61, 32-45.	0.9	35
45	Microwave imaging from experimental data within a Bayesian framework with realistic random noise. Inverse Problems, 2009, 25, 024005.	1.0	34
46	THE DIGITAL WAVE-PROCESSING EXPERIMENT ON CLUSTER. Space Science Reviews, 1997, 79, 209-231.	3.7	32
47	Total electron content in the Martian atmosphere: A critical assessment of the Mars Express MARSIS data sets. Journal of Geophysical Research: Space Physics, 2015, 120, 2166-2182.	0.8	32
48	On origin of outshifted plasma lines during HF modification experiments. Journal of Geophysical Research, 1997, 102, 27265-27269.	3.3	30
49	A two dimensional simulation of the CONSERT experiment (radio tomography of comet Wirtanen). Advances in Space Research, 1999, 24, 1127-1138.	1.2	30
50	Plasma line measurements at Chatanika with highâ€speed correlator and filter bank. Journal of Geophysical Research, 1980, 85, 2998-3012.	3.3	29
51	Detectability of subsurface interfaces in lunar maria by the LRS/SELENE sounding radar: Influence of mineralogical composition. Geophysical Research Letters, 2010, 37, .	1.5	29
52	Jupiter ICY moon explorer (JUICE): Advances in the design of the radar for Icy Moons (RIME). , 2015, , .		29
53	A porosity gradient in 67P/C-G nucleus suggested from CONSERT and SESAME-PP results: an interpretation based on new laboratory permittivity measurements of porous icy analogues. Monthly Notices of the Royal Astronomical Society, 2016, 462, S89-S98.	1.6	29
54	Observations of smallâ€scale plasma density depletions in Arecibo HF Heating Experiments. Journal of Geophysical Research, 1987, 92, 4629-4637.	3.3	28

Wlodek Kofman

#	Article	IF	CITATIONS
55	GPR, a ground-penetrating radar for the Netlander mission. Journal of Geophysical Research, 2003, 108,	3.3	28
56	MARSIS surface reflectivity of the south residual cap of Mars. Icarus, 2009, 201, 454-459.	1.1	28
57	Electron heating by plasma waves in the high latitude E-region and related effects: Observations. Advances in Space Research, 1990, 10, 225-237.	1.2	27
58	In situ generation of intense parallel electric fields in the lower ionosphere. Journal of Geophysical Research, 1996, 101, 335-356.	3.3	27
59	Proton transport model in the ionosphere. 2. Influence of magnetic mirroring and collisions on the angular redistribution in a proton beam. Annales Geophysicae, 1998, 16, 1308-1321.	0.6	27
60	The Castalia mission to Main Belt Comet 133P/Elst-Pizarro. Advances in Space Research, 2018, 62, 1947-1976.	1.2	27
61	Rosetta lander Philae: Flight Dynamics analyses for landing site selection and post-landing operations. Acta Astronautica, 2016, 125, 65-79.	1.7	26
62	Neutral atmosphere studies in the altitude range 90–110 km using EISCAT. Journal of Atmospheric and Solar-Terrestrial Physics, 1986, 48, 837-847.	0.9	25
63	On the usefulness of <i>E</i> region electron temperatures and lower <i>F</i> region ion temperatures for the extraction of thermospheric parameters: a case study. Annales Geophysicae, 1999, 17, 1182-1198.	0.6	25
64	Eiscat multipulse technique and its contribution to auroral ionosphere and thermosphere description. Journal of Geophysical Research, 1985, 90, 3520-3524.	3.3	24
65	The GPR experiment on NETLANDER. Planetary and Space Science, 2000, 48, 1161-1180.	0.9	24
66	HF radio wave attenuation due to a meteoric layer in the atmosphere of Mars. Geophysical Research Letters, 2001, 28, 3039-3042.	1.5	24
67	The EISCAT mesospheric measurements during the CAMP campaign. Journal of Atmospheric and Solar-Terrestrial Physics, 1984, 46, 565-575.	0.9	23
68	Homogeneity of 67P/Churyumov-Gerasimenko as seen by CONSERT: implication on composition and formation. Astronomy and Astrophysics, 2019, 630, A6.	2.1	23
69	Electron temperature measurements by the plasma line technique at the French Incoherent Scatter Radar Facilities. Journal of Geophysical Research, 1981, 86, 6795-6801.	3.3	21
70	STARE and EISCAT measurements: Evidence for the limitation of STARE Doppler velocity observations by the ion acoustic velocity. Journal of Geophysical Research, 1990, 95, 19131-19135.	3.3	21
71	The CONSERT instrument for the ROSETTA mission. Advances in Space Research, 1999, 24, 1115-1126.	1.2	21
72	Computing lowâ€frequency radar surface echoes for planetary radar using Huygensâ€Fresnel's principle. Radio Science, 2015, 50, 1097-1109.	0.8	21

Wlodek Kofman

#	Article	IF	CITATIONS
73	CONSERT constrains the internal structure of 67P at a few metres size scale. Monthly Notices of the Royal Astronomical Society, 2017, 469, S805-S817.	1.6	21
74	Auroral plasma lines: A first comparison of theory and experiment. Journal of Geophysical Research, 1981, 86, 199-205.	3.3	20
75	Comparison between EISCAT UHF and VHF backscattering cross section. Journal of Geophysical Research, 1996, 101, 2369-2376.	3.3	19
76	lonospheric composition measurement by EISCAT using a global fit procedure. Annales Geophysicae, 1996, 14, 1496-1505.	0.6	19
77	Generation of atmospheric gravity waves associated with auroral activity in the polarFregion. Journal of Geophysical Research, 2001, 106, 18543-18554.	3.3	18
78	Philae localization from CONSERT/Rosetta measurement. Planetary and Space Science, 2015, 117, 475-484.	0.9	18
79	Radar Signal Propagation and Detection Through Ice. Space Science Reviews, 2010, 153, 249-271.	3.7	17
80	Characterization of the permittivity of controlled porous water ice-dust mixtures to support the radar exploration of icy bodies. Journal of Geophysical Research E: Planets, 2016, 121, 2426-2443.	1.5	17
81	Experimental evidence of nonâ€isotropic temperature distributions of ions observed by EISCAT in the auroral Fâ€region. Geophysical Research Letters, 1984, 11, 519-522.	1.5	16
82	Variability in ionospheric total electron content at Mars. Planetary and Space Science, 2013, 86, 117-129.	0.9	16
83	The Global Search for Liquid Water on Mars from Orbit: Current and Future Perspectives. Life, 2020, 10, 120.	1.1	16
84	Co-ordinated EISCAT-MICADO interferometer measurements of neutral winds and temperatures in E- and F-regions. Journal of Atmospheric and Solar-Terrestrial Physics, 1990, 52, 625-636.	0.9	15
85	Mapping of overspread targets in radar astronomy. Radio Science, 1991, 26, 403-416.	0.8	15
86	Heat flow effect on the plasma line frequency. Journal of Geophysical Research, 1993, 98, 6079-6085.	3.3	15
87	Neutral dynamics of the high latitude E region from EISCAT measurements: a new approach. Journal of Atmospheric and Solar-Terrestrial Physics, 1996, 58, 121-138.	0.9	15
88	A search for the location of the HF excitation of enhanced ion acoustic and langmuir waves with eiscat and the tromsÃ, heater. Radiophysics and Quantum Electronics, 1999, 42, 533-543.	0.1	15
89	Generation of the lower-thermospheric vertical wind estimated with the EISCAT KST radar at high latitudes during periods of moderate geomagnetic disturbance. Annales Geophysicae, 2008, 26, 1491-1505.	0.6	15
90	Large asymmetric polar scarps on Planum Australe, Mars: Characterization and evolution. Icarus, 2011, 212, 96-109.	1.1	15

#	Article	IF	CITATIONS
91	lon composition measurements and modelling at altitudes from 140 to 350 km using EISCAT measurements. Annales Geophysicae, 1998, 16, 1159-1168.	0.6	14
92	A study on Ganymede's surface topography: Perspectives for radar sounding. Planetary and Space Science, 2013, 77, 40-44.	0.9	14
93	Observations of gravity waves in the auroral zone. Radio Science, 1983, 18, 1059-1065.	0.8	13
94	Electron energy budget in the highâ€latitude ionosphere during Viking/Eiscat coordinated measurements. Journal of Geophysical Research, 1990, 95, 6081-6092.	3.3	13
95	Evidence of anisotropic temperatures of molecular ions in the auroral ionsphere. Geophysical Research Letters, 1991, 18, 163-166.	1.5	13
96	Mars 96 GPR program. Journal of Applied Geophysics, 1995, 33, 27-37.	0.9	13
97	Determination of the ice dielectric permittivity using the data of the test in Antarctica of the ground-penetrating radar for Mars'98 mission. IEEE Transactions on Geoscience and Remote Sensing, 1997, 35, 1338-1349.	2.7	13
98	Photoelectron distribution determination from plasma line intensity measurements obtained at Nancay (France). Planetary and Space Science, 1977, 25, 123-133.	0.9	12
99	Determination of low energy photoelectron distribution from plasma line measurements at Saint Santin. Planetary and Space Science, 1980, 28, 661-673.	0.9	12
100	Observation by the incoherent scatter technique of the hot spots in the auroral zone ionosphere. Geophysical Research Letters, 1987, 14, 1158-1161.	1.5	12
101	Permittivity measurements of porous matter in support of investigations of the surface and interior of 67P/Churyumov-Gerasimenko. Astronomy and Astrophysics, 2015, 583, A39.	2.1	12
102	The morphology of the topside ionosphere of Mars under different solar wind conditions: Results of a multi-instrument observing campaign by Mars Express in 2010. Planetary and Space Science, 2016, 120, 24-34.	0.9	12
103	A radar package for asteroid subsurface investigations: Implications of implementing and integration into the MASCOT nanoscale landing platform from science requirements to baseline design. Acta Astronautica, 2019, 156, 317-329.	1.7	12
104	The interior of Comet 67P/C–G; revisiting CONSERT results with the exact position of the Philae lander. Monthly Notices of the Royal Astronomical Society, 2020, 497, 2616-2622.	1.6	12
105	The Basal Detectability of an Iceâ \in covered Mars by MARSIS. Geophysical Research Letters, 2022, 49, .	1.5	12
106	Generation of 3-D Synthetic Data for the Modeling of the CONSERT Experiment (The Radiotomography) Tj ETQq(709-716.) 0 0 rgBT 3.1	/Overlock 10 11
107	The CONSERT operations planning process for the Rosetta mission. Acta Astronautica, 2016, 125, 212-233.	1.7	11

108Ground penetrating radar sounding of a temperate glacier; modelling of a multilayered medium1.1.010108

#	Article	IF	CITATIONS
109	A priori information required for a two or three dimensional reconstruction of the internal structure of a comet nucleus (consert experiment). Advances in Space Research, 2002, 29, 715-724.	1.2	10
110	Internal structure of Near-Earth Objects. Comptes Rendus Physique, 2005, 6, 321-326.	0.3	10
111	MoMo: a new empirical model of the Mars ionospheric total electron content based on Mars Express MARSIS data. Journal of Space Weather and Space Climate, 2019, 9, A36.	1.1	10
112	Data set generation and inversion simulation of radio waves propagating through a two-dimensional comet nucleus (CONSERT experiment). Radio Science, 2002, 37, 3-1-3-16.	0.8	9
113	Three-dimensional reconstruction of a comet nucleus by optimal control of Maxwell's equations: A contribution to the experiment CONSERT onboard space craft Rosetta. , 2010, , .		9
114	Appearance of layered structures in numerical simulations of polydisperse bodies accretion: Application to cometary nuclei. Icarus, 2011, 213, 369-381.	1.1	9
115	The influence of filtration and decomposition window size on the threshold value and accuracy of land-cover classification of polarimetric SAR images. International Journal of Remote Sensing, 2016, 37, 212-228.	1.3	9
116	Oversampled Pulse Compression Based on Signal Modeling: Application to CONSERT/Rosetta Radar. IEEE Transactions on Geoscience and Remote Sensing, 2017, 55, 2225-2238.	2.7	9
117	Imaging the interior of a comet from bistatic microwave measurements: Case of a scale comet model. Advances in Space Research, 2018, 62, 1977-1986.	1.2	9
118	The search campaign to identify and image the Philae Lander on the surface of comet 67P/Churyumov-Gerasimenko. Acta Astronautica, 2019, 157, 199-214.	1.7	9
119	Multi-temporal phenological indices derived from time series Sentinel-1 images to country-wide crop classification. International Journal of Applied Earth Observation and Geoinformation, 2022, 107, 102683.	1.4	9
120	Electron velocity distribution function in a plasma with temperature gradient and in the presence of suprathermal electrons: application to incoherent-scatter plasma lines. Annales Geophysicae, 1998, 16, 1226-1240.	0.6	8
121	A spaceborne ground penetrating radar: MIMOSA. , 0, , .		8
122	Antennas for sounding of a cometary nucleus in the ROSETTA mission. , 2001, , .		8
123	Top layers charaterization of the Martian surface: Permittivity estimation based on geomorphology analysis. Planetary and Space Science, 2006, 54, 337-344.	0.9	8
124	The equivalent slab thickness of Mars' ionosphere: Implications for thermospheric temperature. Geophysical Research Letters, 2015, 42, 3560-3568.	1.5	8
125	Orbital bistatic radar observations of asteroid Vesta by the Dawn mission. Nature Communications, 2017, 8, 409.	5.8	8
126	An HF bi-phase shift keying radar: application to ice sounding in Western Alps and Spitsbergen glaciers. IEEE Transactions on Geoscience and Remote Sensing, 1992, 30, 1025-1033.	2.7	7

#	Article	IF	CITATIONS
127	Source separation using higher order statistics. Journal of Atmospheric and Solar-Terrestrial Physics, 1992, 54, 1217-1226.	0.9	7
128	Auroral ionospheric and thermospheric measurements using the incoherent scatter technique. Surveys in Geophysics, 1992, 13, 551-571.	2.1	7
129	MEP (Mars Environment Package): toward a package for studying environmental conditions at the surface of Mars from future lander/rover missions. Advances in Space Research, 2004, 34, 1702-1709.	1.2	7
130	A new scenario for the measurement of the auroral plasma parameters in the nonâ€Maxwellian state. Geophysical Research Letters, 1993, 20, 2691-2694.	1.5	6
131	A short review on the F1-region ion composition in the auroral and polar ionosphere. Advances in Space Research, 2006, 37, 913-918.	1.2	6
132	Mars 96 GPR program. , 1995, 33, 27-27.		6
133	Incoherent scatter measurements in the F1-region. Journal of Atmospheric and Solar-Terrestrial Physics, 1986, 48, 857-866.	0.9	5
134	Effects of atmospheric oscillations on the field-aligned ion motions in the polar F-region. Annales Geophysicae, 2000, 18, 1154-1163.	0.6	5
135	Radar techniques to study subsurfaces and interiors of the solar system objects. , 2012, , .		5
136	An interpretation of ion composition diurnal variation deduced from EISCAT observations. Annales Geophysicae, 2001, 19, 351-358.	0.6	5
137	The F- and E-region studies by incoherent scatter radar. Advances in Space Research, 1989, 9, 7-17.	1.2	4
138	Non-thermal ionospheric plasma studies using the incoherent scatter technique. Journal of Atmospheric and Solar-Terrestrial Physics, 1996, 58, 965-978.	0.9	4
139	Rosetta rendezvous and CONSERT operations in 2014: A chimeric surface model of 67P/Churyumov Gerasimenko. Planetary and Space Science, 2012, 67, 84-91.	0.9	4
140	Operation of CONSERT aboard Rosetta during the descent of Philae. Planetary and Space Science, 2013, 89, 151-158.	0.9	4
141	CONSERT line-of-sight link budget simulator. Planetary and Space Science, 2015, 111, 55-61.	0.9	4
142	Observations of the surface of Titan by the Radar Altimeters on the Huygens Probe. Icarus, 2016, 270, 248-259.	1.1	4
143	Reconstruction of the flight and attitude of Rosetta's lander Philae. Acta Astronautica, 2017, 140, 509-516.	1.7	4
144	Post-rendezvous radar properties of comet 67P/CG from the Rosetta Mission: understanding future Earth-based radar observations and the dynamical evolution of comets. Monthly Notices of the Royal Astronomical Society, 2019, 489, 1667-1683.	1.6	4

#	Article	IF	CITATIONS
145	lonosphere of Mars during the consecutive solar minima 23/24 and 24/25 as seen by MARSIS-Mars Express. Icarus, 2023, 393, 114616.	1.1	4
146	3D Time-domain electromagnetic full waveform inversion in Debye dispersive medium accelerated by multi-GPU paralleling. Computer Physics Communications, 2021, 265, 108002.	3.0	4
147	How the Saint Santin incoherent scatter system paved the way for a French involvement in EISCAT. History of Geo- and Space Sciences, 2013, 4, 97-103.	0.1	4
148	Multi-temporal polarimetry in land-cover classification. International Journal of Remote Sensing, 2018, 39, 8182-8199.	1.3	3
149	A new method for determining the total electron content in Mars' ionosphere based on Mars Express MARSIS data. Planetary and Space Science, 2020, 182, 104812.	0.9	3
150	Towards Asteroid Tomography: Modellings and Measurements Using an Analogue Model. , 2020, , .		3
151	Ultraâ€Wideband SAR Tomography on Asteroids. Radio Science, 2021, 56, e2020RS007186.	0.8	3
152	Alternating-code experiment for plasma-line studies. Annales Geophysicae, 1996, 14, 1473.	0.6	3
153	Peering inside near-Earth objects with radio tomography. , 2004, , 201-233.		3
154	Preliminary results on the theory and practice of the measurement of ULF waves in the time-frequency domain. Physics of the Earth and Planetary Interiors, 1976, 12, 135-141.	0.7	2
155	Étude théorique et expérimentale du système corrélo-filtre. Annales Des Telecommunications/Annals of Telecommunications, 1982, 37, 115-122.	1.6	2
156	Alternating-code experiment for plasma-line studies. Annales Geophysicae, 1996, 14, 1473-1479.	0.6	2
157	Incoherent scatter technique applied to study the terrestrial ionosphere and thermosphere. Physics and Chemistry of the Earth, Part C: Solar, Terrestrial and Planetary Science, 2000, 25, 555-562.	0.2	2
158	The ISHTAR Mission: Probing the Internal Structure of NEOs. Highlights of Astronomy, 2005, 13, 738-742.	0.0	2
159	Rosetta CONSERT Data as a Testbed for In Situ Navigation of Space Probes and Radiosciences in Orbit/Escort Phases for Small Bodies of the Solar System. Remote Sensing, 2021, 13, 3747.	1.8	2
160	Angular and radial sampling criteria for monostatic and bistatic radar tomography of solar system small bodies. Advances in Space Research, 2021, 68, 3903-3924.	1.2	2
161	Auroral ionospheric conductivities: a comparison between experiment and modeling, and theoretical f. Annales Geophysicae, 1996, 14, 1297.	0.6	2
162	<i>Letter to the Editor</i> Effects of hot oxygen in the ionosphere: <i>TRANSCAR</i> simulations. Annales Geophysicae, 2001, 19, 257-261.	0.6	2

#	Article	IF	CITATIONS
163	On the usefulness of. Annales Geophysicae, 1999, 17, 1182.	0.6	2
164	SPRATS: a versatile Simulation and Processing RAdar ToolS for planetary missions. , 2020, , .		2
165	Comment on "The effect of strong velocity shears on incoherent scatter spectra: A new interpretation of unusual high latitude spectra― Geophysical Research Letters, 1989, 16, 337-338.	1.5	1
166	Effects of auroral arcs on the generation of gravity waves in the auroral F-region. Advances in Space Research, 2001, 27, 1767-1772.	1.2	1
167	Marsis radar signal simulation. , 0, , .		1
168	Surface echo reduction by clutter simulation, application to the Marsis data. , 2009, , .		1
169	PSTD-based approach to a large-scale inverse scattering problem. , 2011, , .		1
170	Imaging of a scaled comet model from lab experiments. , 2014, , .		1
171	Simulation of SAR images of urban areas by using the ray tracing method with measured values of backscatter coefficients. International Journal of Remote Sensing, 2018, 39, 2671-2689.	1.3	1
172	Multi-Temporal Indices Derived from Time Series of Sentinel-1 Images as a Phenological Description of Plants Growing for Crop Classification. , 2019, , .		1
173	Asteroids Inside Out: Radar Tomography. , 2021, 53, .		1
174	lonospheric composition measurement by EISCAT using a global fit procedure. Annales Geophysicae, 1996, 14, 1496.	0.6	1
175	The Comet Nucleus Sounding Experiment by Radio-wave Transmission (CONSERT). , 2009, , 1-17.		1
176	Performances of the Passive SAR Imaging of Jupiter's Icy Moons. IEEE Transactions on Geoscience and Remote Sensing, 2022, 60, 1-13.	2.7	1
177	Determination of Ice Thicknesses and Properties from H.F. Phase Shift Keying Radar Data. , 0, , .		0
178	Theoretical and computer simulation study of the "Correlofiltre" adaptative system for non stationary processes. , 0, , .		0
179	Adaptive Estimator of a Filter and Its Inverse. IEEE Transactions on Communications, 1985, 33, 1281-1284.	4.9	0

#	Article	IF	CITATIONS
181	Energy deposition in the E and F regions of the high-latitude ionosphere. Advances in Space Research, 1992, 12, 137-146.	1.2	0
182	Foreword, Eighth EISCAT Workshop. Annales Geophysicae, 1998, 16, 1137-1137.	0.6	0
183	<title>GPR on Mars NetLander</title> . , 2000, 4084, 737.		0
184	Simulation of the consert instrument of the Rosetta mission. Advances in Space Research, 2002, 29, 1209-1214.	1.2	0
185	Calibration of the CONSERT/ROSETTA radar. , 0, , .		0
186	The CONSERT operations planning process for the Rosetta mission. , 2018, , .		0
187	Imaging the interior of small Solar bodies: towards a quantitative approach. , 2019, , .		0
188	EI + FWI Method for Reconstructing Interior Structure of Asteroid Using Lander-to-Orbiter Bistatic Radar System. IEEE Transactions on Geoscience and Remote Sensing, 2022, 60, 1-16.	2.7	0
189	Time analysis for a bistatic radar for asteroid tomography: simulations and test bench. CEAS Space Journal, 2021, 13, 653-664.	1.1	0
190	Radar Signal Propagation and Detection Through Ice. Space Sciences Series of ISSI, 2010, , 247-269.	0.0	0
191	Imaging the inner structure of a comet from few measurements in a bistatic scenario: case of a scale model , 2018, , .		Ο